Eur. Phys. J. C 51, 347–358 (2007)
DOI 10.1140/epjc/s10052-007-0298-3

THE EUROPEAN PHYSICAL JOURNAL C

Regular Article – Theoretical Physics

Coulomb gauge approach to $q\bar{q}g$ hybrid mesons

I.J. General[1], F.J. Llanes-Estrada[2,a], S.R. Cotanch[1]

[1] Department of Physics, North Carolina State University, Raleigh, North Carolina 27695-8202, USA
[2] Departamento de Física Teórica I, Universidad Complutense, 28040 Madrid, Spain

Received: 13 February 2007 / Revised version: 16 March 2007 /
Published online: 22 May 2007 –

Abstract. An effective Coulomb gauge Hamiltonian, $H_{\rm eff}$, is used to calculate the light ($u\bar{u}g$), strange ($s\bar{s}g$) and charmed ($c\bar{c}g$) hybrid meson spectra. For the same two parameter $H_{\rm eff}$ providing glueball masses consistent with lattice results and a good description of the observed u, d, s and c quark mesons, a large-scale variational treatment predicts that the lightest hybrid has $J^{PC} = 0^{++}$ and mass 2.1 GeV. The lightest exotic 1^{-+} state is just above 2.2 GeV, near the upper limit of lattice and flux tube predictions. These theoretical formulations all indicate that the observed 1^{-+} $\pi_1(1600)$ and, more clearly, $\pi_1(1400)$ are not hybrid states. The Coulomb gauge approach further predicts that in the strange and charmed sectors, respectively, the ground state hybrids have 1^{+-} with masses 2.1 and 3.8 GeV, while the first exotic 1^{-+} states are at 2.4 and 4.0 GeV. Finally, using our hybrid wavefunctions and the Franck–Condon principle, a novel experimental signature is presented to assist heavy hybrid meson searches.

PACS. 12.39.Mk; 12.39.Pn; 12.39.Ki; 12.40.Yx

1 Introduction

Following the "eightfold way" (Gell-Mann and Ne'eman), the "quark model" (Gell-Mann and Zweig), along with subsequent extensions, has generally explained the observed hadronic spectrum. This is especially true for heavy flavored mesons where certain corrections can be ignored. Even in the light sector, the phenomenological quark model works reasonably well. However, the existence of hadrons with exotic quantum numbers (i.e. J^{PC} states not possible in $q\bar{q}$ or qqq systems) clearly reveals that this model is not complete. It is also expected that there are exotic hadrons with conventional quantum numbers that also cannot be described by the quark model, e.g., glueballs gg, hybrid mesons $q\bar{q}g$ and tetraquarks $q\bar{q}q\bar{q}$.

Possible experimental evidence for a 1^{-+} exotic state was first reported in 1988 [1], but the situation was not clarified until several years later. Now it is believed that there exist two states with these quantum numbers below 2 GeV: $\pi_1(1400)$ [2,3] and $\pi_1(1600)$ [4,5] (note that a recent analysis [6] finds no evidence for either candidate). There are also other reported hybrid candidates with $J^{PC} = 0^{-+}$ [7,8], 1^{--} [9] and 2^{-+} [10–12].

Theoretically, the structure of the π_1 states remains unclear. They could be hybrid or tetraquark mesons, with most theoretical studies [13,14] investigating the former. Lattice gauge simulations [15–19] predict that the lightest hybrid meson is between 1.7 and 2.1 GeV, and results from the flux tube model [20–22] also span much of this range. Only the vintage Bag model [23–29] calculations yield a lower mass, between 1.3 and 1.8 GeV, but [30] argues that the $\pi_1(1400)$ is not a hybrid. Table 1 lists predictions for the u/d, s and c 1^{-+} hybrid mesons.

In this work, we study $q\bar{q}g$ hybrid states using a field theoretical, relativistic many-body approach based upon an effective QCD Hamiltonian, $H_{\rm eff}$, formulated in the Coulomb gauge. This model successfully describes the meson spectrum [34,35] and is also consistent [36] with lattice glueball (and oddball) predictions. Using standard bare current quark masses, it properly incorporates chiral symmetry, yet dynamically generates a constituent mass and spontaneous chiral symmetry breaking [37]. Further, it provides a good description of the vacuum properties (quark and gluon condensates) and respects the global, internal symmetries of QCD, as well as the spatial Euclidean group, all within a minimal two parameter theory. Our work also extends an earlier hybrid calculation [44]

Table 1. Published predicted 1^{-+} masses, in GeV, for light, strange and charmed hybrid mesons

Model [reference]	u/d hybrid	s hybrid	c hybrid
Lattice QCD [15–19, 31–33]	1.7–2.1	1.9	4.2–4.4
Flux tube [20–22]	1.8–2.1	2.1–2.3	4.1–4.5
Bag model [23–29]	1.3–1.8		3.9

[a] e-mail: fllanes@fis.ucm.es

by including previously omitted terms in the Hamiltonian and by comprehensively predicting the light, strange and charmed hybrid meson spectra.

This paper is organized into eight sections. In Sects. 2 and 3 our model Hamiltonian, an approximation to the exact QCD Hamiltonian, is presented along with an improved hyperfine interaction that provides realistic spin splittings in both light and heavy mesons [35] and, for the first time, the non-abelian contributions from the color magnetic fields. Section 4 details the corresponding improved quark and gluon gap equations and a variational formulation for the hybrid meson problem is developed in Sect. 5. Calculations and new results are discussed in Sect. 6, while in Sect. 7 we develop a novel experimental signature for observing hybrid mesons having both conventional and exotic quantum numbers. Finally, we summarize our results and conclusions in Sect. 8.

2 Effective Hamiltonian

The exact QCD Hamiltonian in the Coulomb gauge [45] is (summation over repeated indices is used throughout this paper)

$$H_{\rm QCD} = H_q + H_g + H_{qg} + H_{\rm C}\,, \tag{1}$$

$$H_q = \int {\rm d}x \Psi^\dagger(x)[-{\rm i}\alpha\cdot\nabla + \beta m]\Psi(x)\,, \tag{2}$$

$$H_g = \frac{1}{2}\int {\rm d}x \left[\mathcal{J}^{-1}\mathbf{\Pi}^a(x)\cdot\mathcal{J}\mathbf{\Pi}^a(x) + \mathbf{B}^a(x)\cdot\mathbf{B}^a(x)\right]\,, \tag{3}$$

$$H_{qg} = g\int {\rm d}x \mathbf{J}^a(x)\cdot\mathbf{A}^a(x)\,, \tag{4}$$

$$H_{\rm C} = -\frac{g^2}{2}\int {\rm d}x\,{\rm d}y \rho^a(x)\mathcal{J}^{-1}K^{ab}(\mathbf{x},\mathbf{y})\mathcal{J}\rho^b(y)\,. \tag{5}$$

Here g is the QCD coupling, Ψ is the quark field with current quark mass m, $\mathbf{A}^a$ are the gluon fields satisfying the transverse gauge condition, $\nabla\cdot\mathbf{A}^a = 0$, $a = 1, 2, \ldots, 8$, and $\mathbf{\Pi}^a$ are the conjugate fields, and $\mathbf{B}^a$ are the non-abelian magnetic fields

$$\mathbf{B}^a = \nabla\times\mathbf{A}^a + \frac{1}{2}gf^{abc}\mathbf{A}^b\times\mathbf{A}^c\,. \tag{6}$$

The color densities, $\rho^a(x)$, and quark color currents, $\mathbf{J}^a$, are related to the fields by

$$\rho^a(x) = \Psi^\dagger(x)T^a\Psi(x) + f^{abc}\mathbf{A}^b(x)\cdot\mathbf{\Pi}^c(x)\,, \tag{7}$$

$$\mathbf{J}^a = \Psi^\dagger(x)\alpha T^a\Psi(x)\,, \tag{8}$$

where $T^a = \frac{\lambda^a}{2}$ and f^{abc} are the SU(3) color matrices and structure constants, respectively. The Faddeev–Popov determinant, $\mathcal{J} = \det(\mathcal{M})$, of the matrix $\mathcal{M} = \nabla\cdot\mathbf{D}$, with covariant derivative $\mathbf{D}^{ab} = \delta^{ab}\nabla - gf^{abc}\mathbf{A}^c$, is a measure of the gauge manifold curvature, and the kernel in (5) is given by $K^{ab}(\mathbf{x},\mathbf{y}) = \langle\mathbf{x},a|\mathcal{M}^{-1}\nabla^2\mathcal{M}^{-1}|\mathbf{y},b\rangle$. The Coulomb gauge Hamiltonian is renormalizable, permits resolution of the Gribov problem, preserves rotational invariance, avoids spurious retardation corrections, aids identification of dominant, low energy potentials and does not introduce unphysical degrees of freedom (ghosts) [46].

The bare parton fields have the following normal mode expansions (bare quark spinors u, v, helicity, $\lambda = \pm 1$, and color vectors $\hat{\epsilon}_{\mathcal{C}=1,2,3}$):

$$\Psi(\mathbf{x}) = \int \frac{{\rm d}\mathbf{k}}{(2\pi)^3}\Psi_{\mathcal{C}}(\mathbf{k}){\rm e}^{{\rm i}\mathbf{k}\cdot\mathbf{x}}\hat{\epsilon}_{\mathcal{C}}\,, \tag{9}$$

$$\Psi_{\mathcal{C}}(\mathbf{k}) = u_\lambda(\mathbf{k})b_{\lambda\mathcal{C}}(\mathbf{k}) + v_\lambda(-\mathbf{k})\,{\rm d}^\dagger_{\lambda\mathcal{C}}(-\mathbf{k})\,, \tag{10}$$

$$\mathbf{A}^a(x) = \int \frac{{\rm d}\mathbf{k}}{(2\pi)^3}\frac{1}{\sqrt{2k}}[\mathbf{a}^a(\mathbf{k}) + \mathbf{a}^{a\dagger}(-\mathbf{k})]{\rm e}^{{\rm i}\mathbf{k}\cdot\mathbf{x}}\,, \tag{11}$$

$$\mathbf{\Pi}^a(x) = -{\rm i}\int \frac{{\rm d}\mathbf{k}}{(2\pi)^3}\sqrt{\frac{k}{2}}[\mathbf{a}^a(\mathbf{k}) - \mathbf{a}^{a\dagger}(-\mathbf{k})]{\rm e}^{{\rm i}\mathbf{k}\cdot x}\,, \tag{12}$$

with the Coulomb gauge transverse condition, $\mathbf{k}\cdot\mathbf{a}^a(\mathbf{k}) = (-1)^\mu k_\mu a^a_{-\mu}(\mathbf{k}) = 0$. Here $b_{\lambda\mathcal{C}}(\mathbf{k})$, $d_{\lambda\mathcal{C}}(-\mathbf{k})$ and $a^a_\mu(\mathbf{k})$ ($\mu = 0, \pm 1$) are the bare quark, anti-quark and gluon Fock operators, the latter satisfying the transverse commutation relations,

$$\left[a^a_\mu(\mathbf{k}), a^{b\dagger}_{\mu'}(\mathbf{k}')\right] = (2\pi)^3\delta_{ab}\delta^3(\mathbf{k}-\mathbf{k}')D_{\mu\mu'}(\mathbf{k})\,, \tag{13}$$

with

$$D_{\mu\mu'}(\mathbf{k}) = \delta_{\mu\mu'} - (-1)^\mu\frac{k_\mu k_{-\mu'}}{k^2}\,. \tag{14}$$

Our effective Hamiltonian, $H_{\rm eff}$, follows from $H_{\rm QCD}$ by:

1. replacing the Coulomb kernel in (5) with a calculable confining kernel, i.e.
$$g^2\mathcal{J}^{-1}K^{ab}(\mathbf{x},\mathbf{y})\mathcal{J} \longrightarrow \hat{V}(x,y)\delta_{ab}\,; \tag{15}$$
2. replacing the Faddeev–Popov determinant in (3) by its lowest-order unit value, $\mathcal{J} = \det(\mathcal{M}) \to 1$;
3. approximating the quark–gluon term, (4), by substituting for the gluon vector potential a transverse gluon propagator (kernel) and quark source current having the same color structure
$$H_{qg} \longrightarrow V_T = \frac{1}{2}\int\int {\rm d}\mathbf{x}\,{\rm d}\mathbf{y} J^a_i(\mathbf{x})\hat{U}_{ij}(\mathbf{x},\mathbf{y})J^a_j(\mathbf{y})\,. \tag{16}$$
This is further discussed in the next section, where the form of the kernel $\hat{U}_{ij}(\mathbf{x},\mathbf{y})$ is specified.

Regarding the confining kernel $\hat{V}$, two different forms are employed in this study to provide some measure of the model sensitivity. The first is a simple, phenomenological Cornell type potential,

$$\hat{V}(r = |x-y|) = \hat{V}_{\rm C}(r) + \hat{V}_{\rm L}(r)\,, \tag{17}$$

$$\hat{V}_{\rm C}(r) = -\frac{\alpha_{\rm s}}{r}\,, \tag{18}$$

$$\hat{V}_{\rm L}(r) = \sigma r\,, \tag{19}$$

where the string tension, $\sigma = 0.135\,{\rm GeV}^2$, and $\alpha_{\rm s} = \frac{g^2}{4\pi} = 0.4$ have been previously determined. The Fourier transform of $\hat{V}$ is denoted by V, and in momentum space

these potentials take the form $V_{\rm L}(|\mathbf{p}|) = -8\pi\sigma/p^4$ and $V_{\rm C}(|\mathbf{p}|) = -4\pi\alpha_{\rm s}/p^2$. The other one is a theoretically motivated potential [47] having a renormalization improved short-ranged behavior. This potential was utilized in a previous meson study [35] and has the momentum space representation

$$V(|\mathbf{p}|) = \begin{cases} -\frac{8.04}{p^2}\frac{\ln^{-0.62}\left(\frac{p^2}{m_g^2}+0.82\right)}{\ln^{0.8}\left(\frac{p^2}{m_g^2}+1.41\right)}, & p > m_g\,, \\ -\frac{12.25 m_g^{1.93}}{p^{3.93}}, & p < m_g\,. \end{cases} \quad (20)$$

The parameter m_g sets the string tension and is related to σ by $m_g \cong \sqrt{8\pi\sigma/12.25} \approx 600\,\text{MeV}$.

Due to the above approximations our Coulomb gauge approach is not rigorous QCD but rather a model. However, as mentioned in the introduction, we believe that approximate many-body diagonalizations of $H_{\rm eff}$ capture much of the QCD nature of hadrons, and model predictions should provide a realistic description fruitful for obtaining insight in their structure. There are several reasons supporting this contention. First, the vacuum expectation value of the rigorous Coulomb kernel is known to have approximately the shape of the Cornell potential from lattice studies [38, 39]. Second, we know that confinement manifests itself in this kernel and not in transverse gluon exchange (the H_{qg} term), which is suppressed in the Coulomb gauge by an energy gap (for a recent account see [40]). Third, the connection between the gluon mass gap and the kernel used in this work is based on a simple gap equation (see Sect. 4) where the cutoff plays the role of a dynamical mass counterterm. This treatment is consistent with SU(2) lattice data [41] and is supported by an extended study [47] based on mean field theory and large $N_{\rm c}$ QCD. Fourth, the improved (dressed) quark and gluon degrees of freedom generated by the appropriate gap equations permit a significantly truncated Fock state expansion involving quasi-quarks and quasi-gluons having mass gaps up to order 1 GeV. From energy considerations it follows that the dominant component of the Fock space expansion will therefore contain the minimum number of constituents possible, and mixing with more complex Fock states, which have higher energies, will be suppressed.

One may also examine the role of the cutoff Λ in our calculation. An effective method to incorporate a cutoff in Hamiltonian perturbation theory (valid for this scale being sufficiently high) has been developed for Coulomb gauge QCD using flow equations [42]. This treatment leads to Hamiltonian counterterms to compensate for the suppressed high momentum configurations, saliently the gluon mass gap already discussed above. In a complete renormalization treatment, such counterterms, involving the cutoff or regulating parameter Λ, would be determined by fitting to a known observable. Predictions would then be made with results independent of choice to the observable fitted. We have determined from previous studies [42, 43] that it is possible to effectively bypass this procedure by directly fitting the cutoff parameter to a selected observable. As opposed to the rigorous treatment, this does introduce some cutoff dependence, but the resulting parameter sensitivity is not significant. Consult [34–37] for further details.

3 Hamiltonian g^2 corrections

As mentioned above, a previous hybrid application [44] used this Hamiltonian but set the QCD coupling, g, to zero. This truncation eliminated the quark–gluon interaction, $\mathbf{J}^a \cdot \mathbf{A}^a$, or "hyperfine" term, (4), and also the non-linear (non-Abelian) component of the color magnetic fields, (3) and (6). Now, both are included, so that the non-confining part of the Hamiltonian is consistent to order g^2.

3.1 Hyperfine correction

As explained in [35], the H_{qg} interaction containing the $\mathbf{J}^a \cdot \mathbf{A}^a$ operators is treated perturbatively to second order in g. Then the gluonic operators and intermediate states are modeled with an effective, but non-confining, quark hyperfine interaction with a $\mathbf{J}^a \cdot \mathbf{J}^a$ form. The resulting transverse gluon exchange interaction, specified by (16), retains the same color structure, while its kernel (transverse gluon propagator) reflects the Coulomb gauge

$$\hat{U}_{ij}(\mathbf{x},\mathbf{y}) = \left(\delta_{ij} - \frac{\nabla_i\nabla_j}{\nabla^2}\right)_{\mathbf{x}} \hat{U}(|\mathbf{x}-\mathbf{y}|)\,. \quad (21)$$

The contribution of V_T to the hadron mass is represented by the Feynman diagrams in Fig. 1. For $\hat{U}$ we used the modified Yukawa potential from [35], which is consistent with lattice results [41]. It incorporates a non-zero mass, $m_g = 600\,\text{MeV}$, for the exchanged gluon, that suppresses propagation. Fourier transforming to momentum space, this continuous potential takes the form

$$U(p) = \begin{cases} -\frac{8.04}{p^2}\frac{\ln^{-0.62}\left(\frac{p^2}{m_g^2}+0.82\right)}{\ln^{0.8}\left(\frac{p^2}{m_g^2}+1.41\right)}, & p > m_g\,, \\ -\frac{24.50}{p^2+m_g^2}, & p < m_g\,. \end{cases} \quad (22)$$

Alternative potential forms have also been investigated [35] but found to provide very similar results, provided the transverse gluon propagator is suppressed and matrix elements of the potential have the same value.

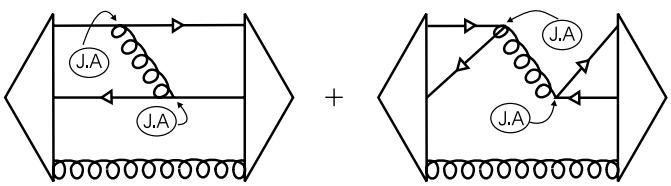

Fig. 1. The hyperfine correction entails the exchange of a gluon between q and $\overline{q}$ and $q\overline{q}$ annihilation

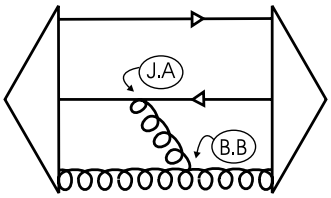

Fig. 2. The non-Abelian correction with triple gluon vertices

3.2 Non-Abelian correction

Similarly, the non-Abelian components of the color magnetic fields, $gf^{abc}\mathbf{A}^b \times \mathbf{A}^c$, in the kinetic energy are also included perturbatively through $(\mathbf{J}^a \cdot \mathbf{A}^a)(\mathbf{B}^a \cdot \mathbf{B}^a)$. The resulting non-Abelian interaction is represented by the Feynman diagram in Fig. 2 and is given by

$$
\begin{aligned}
V_{\mathrm{NA}} = \frac{1}{4}\int\int \mathrm{d}\mathbf{x}\,\mathrm{d}\mathbf{y} f^{abc}\varepsilon_{ijk}\varepsilon_{ilm} \qquad (23)\\
\times \big[J_h^a(\mathbf{y})(\nabla_j^{(\mathbf{x})}\hat{U}_{kh}(\mathbf{x},\mathbf{y}))A_l^b(\mathbf{x})A_m^c(\mathbf{x})\\
+ J_h^b(\mathbf{y})(\nabla_j^{(\mathbf{x})}A_k^a(\mathbf{x}))\hat{U}_{lh}(\mathbf{x},\mathbf{y})A_m^c(\mathbf{x}) \qquad (24)\\
+ J_h^c(\mathbf{y})(\nabla_j^{(\mathbf{x})}A_k^a(\mathbf{x}))A_l^b(\mathbf{x})\hat{U}_{mh}(\mathbf{x},\mathbf{y})\big]\,.
\end{aligned}
$$

where $\hat{U}_{ij}$ is the same kernel as appearing in the hyperfine potential.

4 Gap equation

Having defined the model Hamiltonian, the next step is to calculate the ground state. Since we are free to expand the field operators in any complete basis, we follow the Bardeen–Cooper–Schrieffer (BCS) method and perform a Bogoliubov–Valatin rotation,

$$
\begin{aligned}
B_{\lambda\mathcal{C}}(\mathbf{k}) &= \cos\frac{\theta_k}{2}b_{\lambda\mathcal{C}}(\mathbf{k}) - \lambda\sin\frac{\theta_k}{2}d^\dagger_{\lambda\mathcal{C}}(-\mathbf{k})\,,\\
D_{\lambda\mathcal{C}}(-\mathbf{k}) &= \cos\frac{\theta_k}{2}d_{\lambda\mathcal{C}}(-\mathbf{k}) + \lambda\sin\frac{\theta_k}{2}b^\dagger_{\lambda\mathcal{C}}(\mathbf{k})\,,\\
\alpha^a(\mathbf{k}) &= \cosh\Theta_k\mathbf{a}^a(\mathbf{k}) + \sinh\Theta_k\mathbf{a}^{a\,\dagger}(-\mathbf{k})\,, \qquad (25)
\end{aligned}
$$

which transforms the bare particle operators $\mathbf{a}^a$, $b_{\lambda\mathcal{C}}$ and $d_{\lambda\mathcal{C}}$ into the dressed, quasi-particle operators α^a, $B_{\lambda\mathcal{C}}$ and $D_{\lambda\mathcal{C}}$, respectively. Now the fields are

$$
\begin{aligned}
\Psi_{\mathcal{C}}(\mathbf{k}) &= \mathcal{U}_\lambda(\mathbf{k})B_{\lambda\mathcal{C}}(\mathbf{k}) + \mathcal{V}_\lambda(-\mathbf{k})D^\dagger_{\lambda\mathcal{C}}(-\mathbf{k})\,,\\
\mathbf{A}^a(x) &= \int\frac{\mathrm{d}\mathbf{k}}{(2\pi)^3}\frac{1}{\sqrt{2\omega_k}}[\alpha^a(\mathbf{k}) + \alpha^{a\dagger}(-\mathbf{k})]\mathrm{e}^{\mathrm{i}\mathbf{k}\cdot\mathbf{x}}\,,\\
\mathbf{\Pi}^a(x) &= -\mathrm{i}\int\frac{\mathrm{d}\mathbf{k}}{(2\pi)^3}\sqrt{\frac{\omega_k}{2}}[\alpha^a(\mathbf{k}) - \alpha^{a\dagger}(-\mathbf{k})]\mathrm{e}^{\mathrm{i}\mathbf{k}\cdot x}\,,
\end{aligned}
$$

where $\omega_k = k\mathrm{e}^{-2\Theta_k}$. Note that the dressed quark expansion remains functionally invariant with respect to the bare case, since the quasi-particle spinors have the inverse rotation

$$
\begin{aligned}
\mathcal{U}_\lambda(\mathbf{k}) &= \cos\frac{\theta_k}{2}u_\lambda(\mathbf{k}) - \lambda\sin\frac{\theta_k}{2}v_\lambda(-\mathbf{k})\\
&= \frac{1}{\sqrt{2}}\begin{bmatrix}\sqrt{1+\sin\phi_k}\chi_\lambda\\ \sqrt{1-\sin\phi_k}\sigma\cdot\hat{\mathbf{k}}\chi_\lambda\end{bmatrix}\,, \qquad (26)\\
\mathcal{V}_\lambda(-\mathbf{k}) &= \cos\frac{\theta_k}{2}v_\lambda(-\mathbf{k}) + \lambda\sin\frac{\theta_k}{2}u_\lambda(\mathbf{k})\\
&= \frac{1}{\sqrt{2}}\begin{bmatrix}-\sqrt{1-\sin\phi_k}\sigma\cdot\hat{\mathbf{k}}\chi_\lambda\\ \sqrt{1+\sin\phi_k}\chi_\lambda\end{bmatrix}\,. \qquad (27)
\end{aligned}
$$

Here the quark gap angle, $\phi_k = \phi(k)$, is related to the BCS angle θ_k by $\tan(\phi_k - \theta_k) = m/k$. The quasi-particle (BCS) vacuum, defined by $B_{\lambda\mathcal{C}}|\Omega\rangle = D_{\lambda\mathcal{C}}|\Omega\rangle = \alpha^a_\mu|\Omega\rangle = 0$, is connected to the bare parton one, $b_{\lambda\mathcal{C}}|0\rangle = d_{\lambda\mathcal{C}}|0\rangle = a^a_\mu|0\rangle = 0$, by

$$
\begin{aligned}
|\Omega_{\mathrm{quark}}\rangle &= \mathrm{e}^{-\int\frac{\mathrm{d}\mathbf{k}}{(2\pi)^3}\lambda\tan\frac{\theta_k}{2}b^\dagger_{\lambda\mathcal{C}}(\mathbf{k})d^\dagger_{\lambda\mathcal{C}}(-\mathbf{k})}|0\rangle\\
|\Omega_{\mathrm{gluon}}\rangle &= \mathrm{e}^{-\int\frac{\mathrm{d}\mathbf{k}}{(2\pi)^3}\frac{1}{2}\tanh\Theta_k D_{\mu\mu'}(\mathbf{k})a^{a\dagger}_\mu(\mathbf{k})a^{a\dagger}_{\mu'}(-\mathbf{k})}|0\rangle\,.
\end{aligned}
$$

The BCS vacuum, $|\Omega\rangle = |\Omega_{\mathrm{quark}}\rangle \otimes |\Omega_{\mathrm{gluon}}\rangle$, now contains quark and gluon condensates (correlated $q\bar{q}$ and gg Cooper pairs). Performing a variational minimization of the vacuum expectation value of the Hamiltonian, $\delta\langle\Omega|H_{\mathrm{eff}}|\Omega\rangle = 0$, independently with respect to ϕ_k and ω_k, yields the mass gap equations for each sector:

$$
\begin{aligned}
ks_k - mc_k = \frac{2}{3}\int\frac{\mathrm{d}\mathbf{q}}{(2\pi)^3}\big[&(s_kc_qx - s_qc_k)V(|\mathbf{k}-\mathbf{q}|)\\
&- 2c_ks_qU(|\mathbf{k}-\mathbf{q}|) + 2c_qs_kW(|\mathbf{k}-\mathbf{q}|)\big]\,, \qquad (28)\\
\omega_k^2 = k^2 - \frac{3}{4}\int\frac{\mathrm{d}\mathbf{q}}{(2\pi)^3}V(|\mathbf{k}-\mathbf{q}|)[1+x^2]&\left(\frac{\omega_q^2-\omega_k^2}{\omega_q}\right)\\
&+ \frac{3}{4}g^2\int\frac{\mathrm{d}\mathbf{q}}{(2\pi)^3}\frac{1-x^2}{\omega_q}\,, \qquad (29)
\end{aligned}
$$

where

$$
W(|\mathbf{k}-\mathbf{q}|) \equiv U(|\mathbf{k}-\mathbf{q}|)\frac{x(k^2+q^2) - qk(1+x^2)}{|\mathbf{k}-\mathbf{q}|^2}\,, \qquad (30)
$$

with $s_k = \sin\phi_k$, $c_k = \cos\phi_k$ and $x = \mathbf{k}\cdot\mathbf{q}$. The last term in (29) originates from the non-Abelian component of the gluon kinetic energy. Dimensional analysis of the above integrals reveals that the first equation is UV finite for the linear potential, since $V_{\mathrm{L}}(|\mathbf{p}|) = -8\pi\sigma/p^4$, but not for the Coulomb potential $V_{\mathrm{C}}(|\mathbf{p}|) = -4\pi\alpha_{\mathrm{s}}/p^2$. In (29) there are both logarithmical and quadratical divergences in the UV region and an integration cutoff, $\Lambda = 4$ GeV, determined in previous studies is used.

Once the current quark masses are fixed, the gap equations can be solved numerically for the quark and gluon gap angles. Using $|q\rangle = B_{\lambda\mathcal{C}}(\mathbf{k})^\dagger|\Omega\rangle$ and $|g\rangle = \alpha^a_\mu(\mathbf{k})^\dagger|\Omega\rangle$, the quark and gluon self-energies are respectively

$$
\begin{aligned}
\epsilon_k \equiv \langle q|H_{\mathrm{eff}}|q\rangle &= ms_k + kc_k\\
&- \frac{2}{3}\int\frac{\mathrm{d}\mathbf{q}}{(2\pi)^3}\big[[s_ks_q + c_qc_kx]V(|\mathbf{k}-\mathbf{q}|)\\
&+ 2s_ks_qU(|\mathbf{k}-\mathbf{q}|) + 2c_qc_kW(|\mathbf{k}-\mathbf{q}|)\big] \qquad (31)
\end{aligned}
$$

and, for fixed color index a (no sum),

$$\varepsilon_k^{\mu\mu'} \equiv \langle\Omega|\alpha_\mu^a(\mathbf{k})H_{\rm eff}\alpha_{\mu'}^a(\mathbf{k})^\dagger|\Omega\rangle = \frac{\omega_k^2+k^2}{2\omega_k}\delta_{\mu\mu'} - \frac{3}{4}\int\frac{\mathrm{d}\mathbf{q}}{(2\pi)^3}V(|\mathbf{k}-\mathbf{q}|)\frac{\omega_k^2+\omega_q^2}{\omega_q\omega_k}D_{\mu\mu'}(\mathbf{q}) + \frac{9}{2}g^2\int\frac{\mathrm{d}\mathbf{q}}{(2\pi)^3}\frac{1}{2\omega_k\omega_q} \times\left[2D_{\mu\mu'}(\mathbf{k})-D_{\mu\nu}(\mathbf{k})D_{\nu\nu'}(\mathbf{q})D_{\nu'\mu'}(\mathbf{k})\right], \tag{32}$$

both of which are infrared divergent in the presence of an infrared enhanced kernel. This is a welcome feature of this approach, as colored states are removed from the spectrum. The infrared divergence cancels however in bound state equations for color singlet states leading to a physical spectrum of mesons and baryons.

5 Hybrid mesons

In previous publications [34–37] we have used this model to study the two-body meson and glueball systems by diagonalizing $H_{\rm eff}$ using the Tamm–Dancoff and Random Phase Approximations. We also made predictions for three-body glueballs (oddballs) [36] and published [44] a brief study of the three-body hybrid meson using a variational treatment. We now extend the latter and also provide more complete details of the variational calculation.

5.1 Wavefunction ansatz and quantum numbers

Following our initial study [44], we work in the hybrid center of momentum system, coincident with the BCS frame defining the Coulomb gauge Hamiltonian, and we denote the momenta of the dressed quark, anti-quark and gluon by $\mathbf{q}$, $\bar{\mathbf{q}}$ and $\mathbf{g}$, respectively. We then define $\mathbf{q}_+ \equiv \frac{\mathbf{q}+\overline{\mathbf{q}}}{2}$, $\mathbf{q}_- \equiv q-\overline{q}$ and note that $\mathbf{g} = -\mathbf{q}-\overline{\mathbf{q}} = -2\mathbf{q}_+$.

The color structure of a $q\bar{q}g$ hybrid is determined by the SU(3) algebra:

$$(3\otimes\overline{3})\otimes 8 = (8\oplus 1)\otimes 8 = (8\otimes 8)\oplus(8\otimes 1) = 27\oplus 10\oplus 10\oplus 8\oplus 8\oplus 1\oplus 8\,. \tag{33}$$

Note for an overall color singlet the quarks must be in an octet state like the gluon. As discussed below, this leads to a repulsive $q\bar{q}$ interaction, confirmed by lattice at short range, which increases the mass of the hybrid meson. The hybrid wavefunction will therefore involve the color structure $T^a_{\mathcal{C}_1\mathcal{C}_2}B^\dagger_{\mathcal{C}_1}D^\dagger_{\mathcal{C}_2}\alpha^{a\dagger}$ and has the general form

$$|\Psi^{JPC}\rangle = \int\int\frac{\mathrm{d}\mathbf{q}_+}{(2\pi)^3}\frac{\mathrm{d}\mathbf{q}_-}{(2\pi)^3}\Phi^{JPC}_{\lambda_1\lambda_2\mu}(\mathbf{q}_+,\mathbf{q}_-) \times T^a_{\mathcal{C}_1\mathcal{C}_2}B^\dagger_{\lambda_1\mathcal{C}_1}(\mathbf{q})D^\dagger_{\lambda_2\mathcal{C}_2}(\overline{\mathbf{q}})\alpha^{a\dagger}_\mu(\mathbf{g})|\Omega\rangle\,, \tag{34}$$

which is summed over color and angular momentum magnetic sub-states.

There are five angular momenta in this system, two orbital, $\mathbf{l}_\pm$ (associated with $\mathbf{q}_\pm$), having z projections $m_\pm$, and the three spins, $S_q = S_{\overline{q}} = 1/2$ and $S_g = 1$, with projections λ_1, λ_2 and μ, respectively. To form states with total angular momentum J, with projection m_J, we use the coupling scheme

$$\mathbf{S} = \mathbf{S}_q + \mathbf{S}_{\overline{q}},\ \mathbf{j} = \mathbf{S}_g + \mathbf{l}_+,\ \mathbf{L} = \mathbf{j} + \mathbf{l}_-,\ \mathbf{J} = \mathbf{L} + \mathbf{S}\,.$$

Then with the appropriate Clebsch–Gordan coefficients, the hybrid wavefunction can be expressed in terms of a radial wavefunction $F^{JPC}(q_+,q_-)$ and spherical harmonics, $Y^{m_\pm}_{l_\pm}(\mathbf{q}_\pm)$,

$$\Phi^{JPC}_{\lambda_1\lambda_2\mu}(\mathbf{q}_+,\mathbf{q}_-) = F^{JPC}(q_+,q_-)Y^{m_+}_{l_+}(\hat{\mathbf{q}}_+)Y^{m_-}_{l_-}(\hat{\mathbf{q}}_-) \times(-1)^{\frac{1}{2}-\lambda_2}\left\langle\frac{1}{2}\frac{1}{2},\lambda_1(-\lambda_2)|Sm_S\right\rangle \times(-1)^\mu\langle 1l_+,(-\mu)m_+|jm_j\rangle \times\langle jl_-,m_jm_-|Lm_{\rm L}\rangle\langle LS,m_{\rm L}m_S|JM_J\rangle\,.$$

Since the intrinsic parity for a $q\bar{q}$ pair and a gluon are both -1, and the two orbital parities are $(-1)^{l_-}$ and $(-1)^{l_+}$, the total hybrid meson parity is

$$P = (-1)(-1)(-1)^{l_+}(-1)^{l_-} = (-1)^{l_++l_-}\,. \tag{35}$$

Table 2. Hybrid meson quantum numbers up to $J=3$. Note the exotic states and states forbidden by transversality: $l_+ = 1$ cannot couple to $j = 0$

l_+	l_-	S	j	L	J	P	C	$J^{\rm PC}$	
0	0	0	1	1	1	+	−	1^{+-}	
0	0	1	1	1	0	+	+	0^{++}	
0	0	1	1	1	1	+	+	1^{++}	
0	0	1	1	1	2	+	+	2^{++}	
0	1	0	1	0	0	−	+	0^{-+}	
0	1	0	1	1	1	−	+	1^{-+}	Exotic
0	1	0	1	2	2	−	+	2^{-+}	
0	1	1	1	0	1	−	−	1^{--}	
0	1	1	1	1	0	−	−	0^{--}	Exotic
0	1	1	1	1	1	−	−	1^{--}	
0	1	1	1	1	2	−	−	2^{--}	
0	1	1	1	2	1	−	−	1^{--}	
0	1	1	1	2	2	−	−	2^{--}	
0	1	1	1	2	3	−	−	3^{--}	
1	0	0	0	0	0	−	−	0^{--}	Forbidden
1	0	0	1	1	1	−	−	1^{--}	
1	0	0	2	2	2	−	−	2^{--}	
1	0	1	0	0	1	−	+	1^{-+}	Forbidden
1	0	1	1	1	0	−	+	0^{-+}	
1	0	1	1	1	1	−	+	1^{-+}	Exotic
1	0	1	1	1	2	−	+	2^{-+}	
1	0	1	2	2	1	−	+	1^{-+}	Exotic
1	0	1	2	2	2	−	+	2^{-+}	
1	0	1	2	2	3	−	+	3^{-+}	Exotic

Finally, exchanging all additive quantum numbers, as required by charge conjugation, yields a $(-1)^{l_-+S}$ factor from the space and spinor $q\overline{q}$ components that needs to be combined with the phase of the $q\overline{q}g$ composite color component. Although the gluon octet is not an eigenstate of C-parity, each gluon has a $q\overline{q}$ octet partner with opposite C-parity, resulting in a -1 contribution for the combined $[[3\otimes\bar{3}]_8\otimes 8]_1$ system. Therefore the hybrid C-parity is

$$C=(-1)(-1)^{l_-+S}=(-1)^{1+l_-+S}\,. \tag{36}$$

The extra -1 phase, as compared to a conventional $q\overline{q}$ meson having C-parity $(-1)^{l_-+S}$, is responsible for generating exotic quantum numbers for certain hybrid states (e.g. $J^{PC}=1^{-+}$). Table 2 lists quantum numbers for the model hybrid states for J up to 3. Note the exotic quantum number states and also states forbidden by the Coulomb gauge transversality condition (gluon orbital $l_+=1$ cannot couple with its spin to produce $j=0$).

5.2 Variational equations of motion

We now compute the hybrid mass, M_{JPC}, for each J^{PC} with special interest focusing upon the exotic states. In terms of the above variational wavefunction, the upper bound for the mass is given by

$$\begin{aligned}M_{JPC}&=\frac{\langle\Psi^{JPC}|H_{\rm eff}|\Psi^{JPC}\rangle}{\langle\Psi^{JPC}|\Psi^{JPC}\rangle}\\&=M_{\rm self}+M_{q\overline{q}}+M_{qg}+M_{qgq}+M_{ggg}\,.\end{aligned} \tag{37}$$

Here, the subscripts indicate the mass contribution from the self-energy of the three constituents, $M_{\rm self}$, the $q\overline{q}$ interaction, $M_{q\overline{q}}$, the qg and $\overline{q}g$ interactions, M_{qg}, the second order correction from the qgq and $\overline{q}g\overline{q}$ vertices, M_{qgq}, and the second order correction from triple gluon vertices, M_{ggg}. The three-body expectation value entails twelve dimensional integrals, which can be reduced to nine dimensions by working in the center of momentum. The detailed expressions are

$$\begin{aligned}M_{\rm self}=&\int\!\!\int\frac{{\rm d}\mathbf{q}}{(2\pi)^3}\frac{{\rm d}\overline{\mathbf{q}}}{(2\pi)^3}\\&\times\Phi^{JPC\dagger}_{\lambda_1\lambda_2\mu}(\mathbf{q},\overline{\mathbf{q}})\Phi^{JPC}_{\lambda_1\lambda_2\mu'}(\mathbf{q},\overline{\mathbf{q}})\\&\times\left[D_{\nu\nu'}(\mathbf{g})(\epsilon_{\mathbf{q}}+\epsilon_{\overline{\mathbf{q}}})+D_{\mu\nu}(\mathbf{g})D_{\mu'\nu'}(\mathbf{g})\varepsilon^{\nu\nu'}_{\mathbf{g}}\right],\end{aligned} \tag{38}$$

$$\begin{aligned}M_{q\overline{q}}=&-\frac{1}{2}\int\!\!\int\!\!\int\frac{{\rm d}\mathbf{q}}{(2\pi)^3}\frac{{\rm d}\overline{\mathbf{q}}}{(2\pi)^3}\frac{{\rm d}\mathbf{q}'}{(2\pi)^3}\\&\times\Phi^{JPC\dagger}_{\lambda_1\lambda_2\mu}(\mathbf{q},\overline{\mathbf{q}})\Phi^{JPC}_{\lambda_1'\lambda_2'\mu'}(\mathbf{q}',\mathbf{q}+\overline{\mathbf{q}}-\mathbf{q}')D_{\mu\mu'}(\mathbf{g})\\&\times\left[\frac{1}{3}V(|\mathbf{q}'-\mathbf{q}|)\mathcal{U}^\dagger_{\lambda_1\mathbf{q}}\mathcal{U}_{\lambda_1'\mathbf{q}'}\mathcal{V}^\dagger_{\lambda_2'\mathbf{q}+\overline{\mathbf{q}}-\mathbf{q}'}\mathcal{V}_{\lambda_2\overline{\mathbf{q}}}\right.\\&\left.+V(|\mathbf{q}+\overline{\mathbf{q}}|)\mathcal{U}^\dagger_{\lambda_1\mathbf{q}}\mathcal{V}_{\lambda_2\overline{\mathbf{q}}}\mathcal{V}^\dagger_{\lambda_2'\mathbf{q}+\overline{\mathbf{q}}-\mathbf{q}'}\mathcal{U}_{\lambda_1'\mathbf{q}'}\right],\end{aligned} \tag{39}$$

$$\begin{aligned}M_{qg}=&\frac{3}{4}\int\!\!\int\!\!\int\frac{{\rm d}\mathbf{q}}{(2\pi)^3}\frac{{\rm d}\overline{\mathbf{q}}}{(2\pi)^3}\frac{{\rm d}\mathbf{q}'}{(2\pi)^3}\\&\times\left[\frac{\omega_{q+\overline{q}}+\omega_{q'+\overline{q}}}{\sqrt{\omega_{q+\overline{q}}\omega_{q'+\overline{q}}}}\Phi^{JPC\dagger}_{\lambda_1\lambda_2\mu}(\mathbf{q},\overline{\mathbf{q}})\Phi^{JPC}_{\lambda\lambda_2\mu'}(\mathbf{q}',\overline{\mathbf{q}})\right.\\&\times D_{\mu'\mu''}(\mathbf{q}+\overline{\mathbf{q}})D_{\mu\mu''}(\mathbf{q}+\overline{\mathbf{q}})V(|\mathbf{q}-\mathbf{q}'|)\mathcal{U}^\dagger_{\lambda\mathbf{q}'}\mathcal{U}_{\lambda_1\mathbf{q}}\\&+\frac{\omega_{q+\overline{q}}+\omega_{q+q'}}{\sqrt{\omega_{q+\overline{q}}\omega_{q+q'}}}\Phi^{JPC\dagger}_{\lambda_1\lambda_2\mu}(\mathbf{q},\overline{\mathbf{q}})\Phi^{JPC}_{\lambda_1\lambda\mu'}(\mathbf{q},\mathbf{q}')\\&\left.\times D_{\mu'\mu''}(\mathbf{q}+\mathbf{q}')D_{\mu''\mu}(\mathbf{q}+\overline{\mathbf{q}})V(|\overline{\mathbf{q}}-\mathbf{q}'|)\mathcal{V}^\dagger_{\lambda\mathbf{q}'}\mathcal{V}_{\lambda_2\overline{\mathbf{q}}}\right],\end{aligned} \tag{40}$$

$$\begin{aligned}M_{qgq}=&\frac{1}{2}\int\!\!\int\!\!\int\frac{{\rm d}\mathbf{q}}{(2\pi)^3}\frac{{\rm d}\overline{\mathbf{q}}}{(2\pi)^3}\frac{{\rm d}\mathbf{q}'}{(2\pi)^3}\\&\times\Phi^{JPC\dagger}_{\lambda_1\lambda_2\mu}(\mathbf{q},\overline{\mathbf{q}})\Phi^{JPC}_{\lambda_1'\lambda_2'\mu'}(\mathbf{q}',\mathbf{q}+\overline{\mathbf{q}}-\mathbf{q}')D_{\mu\mu'}(\mathbf{g})\\&\times\left[\frac{1}{3}U_{mn}(\mathbf{q}'-\mathbf{q})\mathcal{U}^\dagger_{\lambda_1\mathbf{q}}\alpha_m\mathcal{U}_{\lambda_1'\mathbf{q}'}\mathcal{V}^\dagger_{\lambda_2'\mathbf{q}+\overline{\mathbf{q}}-\mathbf{q}'}\alpha_n\mathcal{V}_{\lambda_2\overline{\mathbf{q}}}\right.\\&\left.+U_{mn}(\mathbf{q}+\overline{\mathbf{q}})\mathcal{U}^\dagger_{\lambda_1\mathbf{q}}\alpha_m\mathcal{V}_{\lambda_2\overline{\mathbf{q}}}\mathcal{V}^\dagger_{\lambda_2'\mathbf{q}+\overline{\mathbf{q}}-\mathbf{q}'}\alpha_n\mathcal{U}_{\lambda_1'\mathbf{q}'}\right],\end{aligned} \tag{41}$$

$$\begin{aligned}M_{ggg}=&\frac{3}{8}{\rm i}\int\!\!\int\!\!\int\frac{{\rm d}\mathbf{q}}{(2\pi)^3}\frac{{\rm d}\overline{\mathbf{q}}}{(2\pi)^3}\frac{{\rm d}\mathbf{q}'}{(2\pi)^3}\\&\times\frac{1}{\sqrt{\omega_{-q'-\overline{q}}\omega_{q+\overline{q}}}}\Phi^{JPC\dagger}_{\lambda_1\lambda_2\mu}(\mathbf{q},\overline{\mathbf{q}})\Phi^{JPC}_{\lambda_1'\lambda_2\mu'}(\mathbf{q}',\overline{\mathbf{q}})\\&\times\left(\mathcal{U}^\dagger_{\lambda_1\mathbf{q}}\alpha_h\mathcal{U}_{\lambda_1'\mathbf{q}'}+\mathcal{V}^\dagger_{\lambda_1\mathbf{q}}\alpha_h\mathcal{V}_{\lambda_1'\mathbf{q}'}\right)\\&\times\left\{\nabla_l U_{kh}(\mathbf{q}-\mathbf{q}')\Big[D_{\mu k}(\mathbf{g})D_{l\mu'}(-\mathbf{q}'-\overline{\mathbf{q}})\right.\\&\left.-D_{\mu l}(\mathbf{g})D_{k\mu'}(-\mathbf{q}'-\overline{\mathbf{q}})\Big]\right.\\&+{\rm i}(\mathbf{q}-\mathbf{q}')_l U_{lh}(\mathbf{q}'+\mathbf{q})D_{\mu k}(\mathbf{g})D_{k\mu'}(-\mathbf{q}'-\overline{\mathbf{q}})\\&-{\rm i}U_{kh}(\mathbf{q}-\mathbf{q}')\left[(\mathbf{q}'+\overline{\mathbf{q}})_l D_{\mu l}(\mathbf{g})D_{k\mu'}(-\mathbf{q}'-\overline{\mathbf{q}})\right.\\&\left.\left.+(\mathbf{q}+\overline{\mathbf{q}})_l D_{\mu k}(\mathbf{g})D_{l\mu'}(-\mathbf{q}'-\overline{\mathbf{q}})\right]\right\}.\end{aligned} \tag{42, 43}$$

In the above expressions, $\epsilon_{\mathbf{q}}$, $\epsilon_{\overline{\mathbf{q}}}$ and $\varepsilon^{\mu\mu'}_{\mathbf{g}}$ are the quark, anti-quark and gluon self-energies, respectively, evaluated at the indicated momentum ($\mathbf{g}=-\mathbf{q}-\overline{\mathbf{q}}$). A pictorial representation for each type of contribution is given by the Feynman diagrams in Fig. 3.

The above expectation values are then computed variationally using the separable radial wavefunction, $F(q_+,q_-)=f(q_+,\alpha_+)f(q_-,\alpha_-)$, having two variational parameters, α_+ and α_-. We investigated two functional forms for f; a gaussian and a scalable numerical solution from our two-body meson studies. In general, the gaussian radial wavefunction,

$$f(q_\pm,\alpha_\pm)={\rm e}^{-x_\pm^2}\,,\quad x_\pm=\frac{q_\pm}{\alpha_\pm}\,, \tag{44}$$

provided better results (lower variational mass) for s-wave states when compared to the numerical one. This was also true for p-wave orbital excitations, provided the gaussian was multiplied by $x_\pm$ corresponding to $l_\pm=1$. All integrals were calculated using the Monte Carlo method with

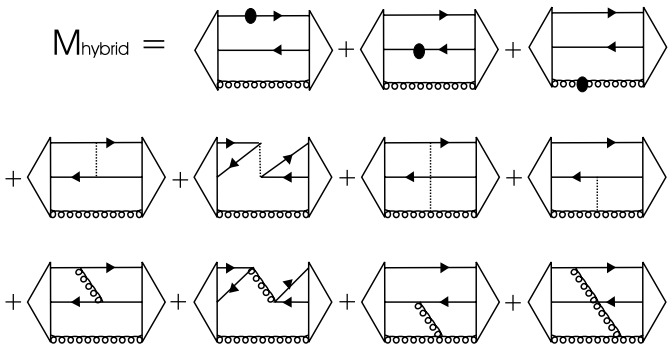

Fig. 3. Diagrams for $\langle \Psi^{JPC} | H_{\rm eff} | \Psi^{JPC} \rangle$

the adaptive sampling algorithm VEGAS [48, 49]. The integrals were evaluated several times with an increasing number of points until there was convergence. The hybrid mass error introduced by this procedure is about ± 50 MeV. For each J^{PC} hybrid state we optimized the variational parameters α_+ and α_- to produce the lowest mass. In terms of the string tension, their values fell in the ranges $0.9\sqrt{\sigma} \leq \alpha_+ \leq 1.7\sqrt{\sigma}$ and $1.0\sqrt{\sigma} \leq \alpha_- \leq 3.3\sqrt{\sigma}$.

6 Results: Hybrid meson spectrum

6.1 Light hybrid mesons

For the light hybrid calculation we used $m = 5$ MeV [50] for the u/d current quark mass. Results are listed in Table 3, which shows that the ground state is the 0^{++} non-exotic scalar, followed by the triplet 1^{+-}, 2^{++} and 1^{++}. The lightest hybrid mass is 2.1 GeV.

For exotic states, as can be seen from Table 2, at least one p-wave in $\mathbf{q}_+$ or $\mathbf{q}_-$ is required. Because the $q\bar{q}$ interaction is repulsive for quarks in a color octet state, the excitation energy is less for a l_+ (gluon orbital) excitation than a l_- ($q\bar{q}$ orbital) excitation since the quarks are further separated and experience a larger repulsive linear force.

The lightest exotic state is the $I = 1, 1^{-+}$ state, with mass 2.2 GeV. This is slightly higher than the flux tube model and lattice QCD predicted masses for this state, which were between 1.7 and 2.1 GeV (see Table 1).

We studied the effects from including the non-Abelian (NA) and hyperfine corrections for several states. Generally, both effects were small (except the hyperfine correction for charmed quarks, see below), roughly of the same order as the overall 50 MeV Monte Carlo error. In particular, the NA correction entailed several terms with different signs, which tended to cancel.

Our model exotic spectrum (see Fig. 4) spans almost a GeV, between 2.1 and about 3 GeV and includes predictions for J up to 3. There are no exotic $J = 2$ model states in this region, since they require a d-wave or two p-waves, both involving much higher excitations.

Table 3. Spectrum of light hybrid meson states. Error $\approx \pm 50$ MeV

$(I)J^{\rm PC}$	$M_{J^{\rm PC}}$ (MeV) no corrections	$M_{J^{\rm PC}}$ (MeV) with g^2 corrections	
$(0)0^{++}$	2080	2135	
$(1)0^{++}$	2065	2100	Ground
$(0)1^{+-}$	2135	2140	*
$(1)1^{+-}$	2135	2140	*
$(0)2^{++}$	2340	2335	
$(1)2^{++}$	2180	2170	
$(0)1^{++}$	2415	2470	
$(1)1^{++}$	2110	2170	
$(0)1^{-+}$	2500	2525	Exotic
$(1)1^{-+}$	2205	2220	Exotic
$(0)0^{--}$	2275	2280	Exotic
$(1)0^{--}$	2280	2285	Exotic
$(0)1^{-+}$	2370	2400	Exotic*
$(1)1^{-+}$	2370	2400	Exotic*
$(0)1^{-+}$	2760	2790	Exotic
$(1)1^{-+}$	2570	2600	Exotic
$(0)3^{-+}$	3030	3040	Exotic
$(1)3^{-+}$	2910	2915	Exotic

* Isospin degenerate states

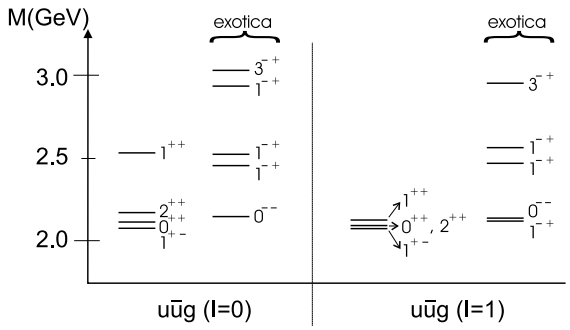

Fig. 4. $u\overline{u}g$ spectrum

Finally, we comment on an interesting isospin splitting effect. From Fig. 3, annihilation terms only contribute to the hybrid mass if the $q\overline{q}$ pair has quantum numbers consistent with the interaction. This is satisfied when $I_{q\overline{q}} = 0$ and $S = 1$. The annihilation diagrams can increase the $I = 0$ hybrid states by several hundred MeV, as detailed in Table 3. In other cases, the 1^{+-} and one of the 1^{-+} states should be isospin degenerate, as we compute to within the Monte Carlo error. On the other hand, the states 0^{++} and 0^{--} are not expected to be degenerate but, within the error, they are. It may be that the isospin splitting is not zero, but rather is smaller than the numerical error. Note that the annihilation process for s-wave, isoscalar quarks in a triplet spin state is analogous to e^-e^+ annihilation in the triplet state of positronium.

6.2 Strange hybrid mesons

Table 4 summarizes results obtained for the $s\bar{s}g$ (hidden strangeness) hybrid mesons using a bare strange quark mass of 80 MeV. Now, the ground state is given by the non-exotic pseudovector state 1^{+-}, with a 2.125 GeV mass, not at all reflecting the 75 MeV additional quark flavor mass contribution (the hybrid calculation is only sensitive to current quark masses above 200 MeV). Our prediction is in good agreement with the flux tube model and slightly above the only lattice prediction (see Table 1). In the exotic sector, the lightest state is given by 0^{--}, with mass 2.3 GeV. Although there are also hybrid states with explicit strangeness, e.g. $s\bar{u}g$, we do not show predictions, since the effect from the s/u quark mass difference is small.

6.3 Heavy hybrid mesons

Table 5 shows the results for the $c\bar{c}g$ (charmonium) hybrid mesons using a charmed quark mass of 1.0 GeV. The ground state is given, again, by the 1^{+-} state, with mass 3.83 GeV, while the lightest exotic hybrid lies at 4.02 GeV. These numbers are in reasonable agreement with previous lattice and flux tube predictions, as listed in Table 1.

Note that the correction introduced in the charmed case by the g^2 terms is roughly 500 to 600 MeV, significantly higher than in the lighter hybrid systems, where the average corrections are 25 to 50 MeV. This large effect arises from the hyperfine correction to the quark and antiquark self-energies (see (31) and (38)), which is enhanced for heavier quark masses as discussed further in [35]. Related, and as illustrated in Fig. 5, the charmonium hybrid spectrum now has a level ordering slightly different from the lighter hybrid spectra.

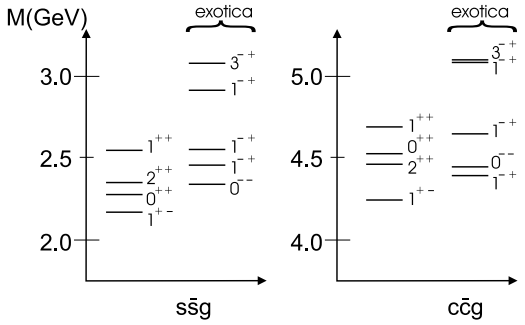

Fig. 5. Low lying $s\bar{s}g$ and $c\bar{c}g$ spectra

6.4 Sensitivity to potential and parameters

One of our key findings using the Cornell potential is that the mass of the lightest hybrid, especially the exotic 1^{-+}, is above 2 GeV. Because of the ramifications of this result for exotic state searches, we have performed an interaction sensitivity study by varying both potential forms and parameters.

We first varied the parameters in the Cornell potential to obtain a lower bound for our predicted exotic hybrid mass. Results are shown in Table 6 for different Coulomb potential parameters, α_s, and string tensions, σ, found in the literature. For any combination of values consistent with previous studies [34–37] it was not possible to reduce the light hybrid mass to 1600 MeV. In particular, we tried $0.0 \leq \alpha_s \leq 0.4$ and $367\,\text{MeV} \leq \sqrt{\sigma} \leq 424\,\text{MeV}$. Indeed, to obtain a hybrid mass as low as 1600 MeV required an unphysical $\sqrt{\sigma} = 262$ MeV.

Table 6 also lists predictions for the confining potential given by (20) for values of the parameter $m_g = \sqrt{8\pi\sigma/12.25}$ corresponding to the two different Cornell

Table 4. Spectrum of $s\bar{s}g$ states. Error $\approx \pm 50$ MeV

J^{PC}	$M_{J^{\text{PC}}}$ (MeV) no corrections	$M_{J^{\text{PC}}}$ (MeV) with g^2 corrections	
1^{+-}	2095	2125	Ground
0^{++}	2045	2140	
2^{++}	2290	2315	
1^{++}	2325	2420	
1^{-+}	2350	2395	Exotic
0^{--}	2270	2300	Exotic
1^{-+}	2440	2485	Exotic
1^{-+}	2760	2820	Exotic
3^{-+}	2995	3030	Exotic

Table 5. Spectrum of $c\bar{c}g$ states. Error $\approx \pm 50$ MeV

J^{PC}	$M_{J^{PC}}$ (MeV) no corrections	$M_{J^{PC}}$ (MeV) with g^2 corrections	
1^{+-}	3310	3830	Ground
0^{++}	3295	3945	
2^{++}	3410	3965	
1^{++}	3450	4100	
1^{-+}	3545	4020	Exotic
0^{--}	3510	4020	Exotic
1^{-+}	3590	4155	Exotic
1^{-+}	3985	4565	Exotic
3^{-+}	4065	4615	Exotic

Table 6. Calculated light and charmonium hybrid 1^{-+} masses, in GeV, using different interactions

potential/parameters	$I = 1$ $u\bar{d}g$ hybrid	$c\bar{c}g$ hybrid
Cornell (2)		
$\sqrt{\sigma} = 367$ MeV, $\alpha_s = 0.4$	2220	4155
$\sqrt{\sigma} = 367$ MeV, $\alpha_s = 0.2$	2390	4415
$\sqrt{\sigma} = 367$ MeV, $\alpha_s = 0.0$	2540	4645
$\sqrt{\sigma} = 424$ MeV, $\alpha_s = 0.4$	2555	4525
Renormalized (20)		
$m_g = 526$ MeV	2705	4730
$m_g = 607$ MeV	3010	5130

string tensions σ but with the same current quark masses ($m_u = 5\,\text{MeV},\ m_c = 1\,\text{GeV}$). Note that this interaction yields $u\bar{d}g$ and $c\bar{c}g$ hybrids that are heavier than those given by the Cornell potential. Most significantly, this potential also predicts the lightest exotic hybrid has mass above 2 GeV. If instead we use $m_c = 0.85\,\text{GeV}$, which provides a reasonable description of the charmonium spectrum, the $1^{-+}c\bar{c}g$ mass decreases to 4815 MeV for $m_g = 607\,\text{MeV}$.

7 Searching for hybrid mesons

Discovering exotic hadrons is a major goal motivating the Jefferson Lab 12 GeV upgrade and is also an important collaborative project at other facilities, such as Babar, Belle, RHIC, etc. For low energy investigations of light quark exotic systems there is, unfortunately, no clean energy scale demarcation, since Λ_{QCD} governs the momentum distributions in light mesons, and the strange quark mass is of the same order of magnitude. The obvious detection strategy is therefore to perform statistically accurate cross sections measurements to extract partial wave amplitudes with explicitly exotic quantum numbers not accessible to ordinary $q\bar{q}$ states. However for (hidden) exotica with conventional meson quantum numbers, it will be difficult to establish their nature. Note that certain flux tube model [20] and lattice predictions indicate that p-wave hybrid mesons prefer to decay to hadron pairs with one hadron also having a p-wave, rather than to two s-wave hadrons with a relative motion p-wave, e.g. ηh_1 in an s-wave as opposed to $\pi\pi$ in a p-wave. It will be interesting to check this prediction experimentally.

For heavier quark systems, however, we propose a novel way to distinguish excited conventional, radially excited quarkonia from hybrid states. The method is based upon the energy scale separation provided by the heavy quark mass and involves two key points. First, we note that, due to the gluon mass gap scale, a conventional $q\bar{q}$ ground state (e.g. a well established J/ψ or Υ, etc.) is lighter than a $q\bar{q}g$ ground state hybrid with the same flavor. Indeed, the ground state hybrid mass is more comparable to a radially excited quarkonium state. For example in our approach the $\psi(4s)$ and the ground state vector $c\bar{c}g$ state have similar masses. Now different eigenstates of a Hermitian Hamiltonian are orthogonal with the nth radial excited state having $n-1$ nodes. Therefore, even though the total energies (masses) are similar, the relative momentum distribution of the quarks in excited charmonium looks quite different from the quark momentum distribution in the ground state hybrid with the same quark flavors (see Figs. 6 and 7).

The second point involves the Franck–Condon (FC) principle widely used in molecular physics. Franck and Condon were the first to appreciate that molecular electronic transitions proceed too rapidly for the much heavier nuclei to respond. The FC principle is applicable whenever there is a mass scale separation between different particles. In the context of quarkonium this means that the light fields (pions, gluons, etc.) quickly rearrange and the heavy quarks do not appreciably change their momentum distribution in the decay. Hence, the relative momentum between the decay products directly correlates with the quark momentum distribution in the parent quarkonium. Unfortunately in the simplest two-body decays such as

$$\psi(ns) \to D\bar{D}\,, \quad \Upsilon(ns) \to B\bar{B}\,,$$

the FC constraint is not relevant, since in the center of mass frame the momentum of the final products is fixed. This leads to smaller wavefunction overlaps, suppressing the decay somewhat. However in three-body decays such as

$$\psi(ns) \to D\bar{D}\pi\,, \quad \Upsilon(ns) \to B\bar{B}\pi\,,$$

the FC constraint applies. The first reaction can be employed to study the recently discovered $\psi(4260)$. The second will be useful in an envisioned Belle collaboration measurement to establish whether this excited bottomonium state is the predicted quark model $5s$ meson state.

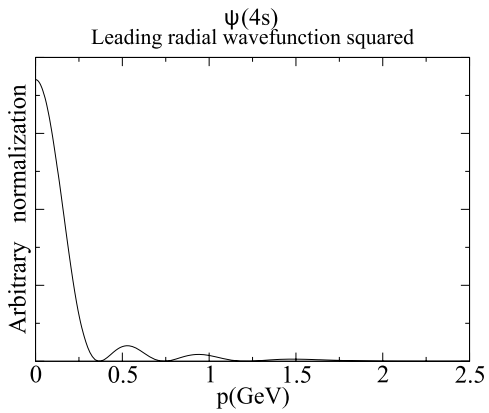

Fig. 6. Probability density, $|\psi(p)|^2$, for the $4s$ charmonium state. This is the relative $c\bar{c}$ quark momentum distribution

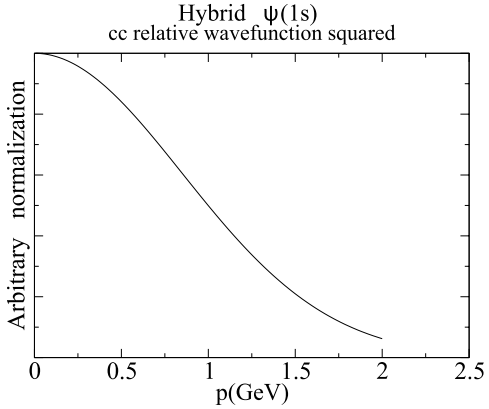

Fig. 7. Typical quark relative momentum distribution in a $c\bar{c}g$ hybrid state with a mass near 4300 MeV. The extra mass energy, relative to a $c\bar{c}$ J/ψ, corresponds to gluon field excitations in collective models such as the flux tube approach or in the quasi-particle (gluon) mass gap in the constituent picture, but not in nodal radial excitation for the relative $c\bar{c}$ motion (compare to the radially excited charmonium distribution in Fig. 6)

Thus, we contend that the relative momentum distribution between the D and $\bar{D}$ mesons in the $D\bar{D}\pi$ system mirrors the momentum distribution of the quarks in the parent ψ meson. Since the hybrid ground state wavefunction does not have a node, the resulting momentum distribution for the $D\bar{D}$ subsystem is also node-less and thus smoother than that for a conventional radially excited charmonium. Including the relevant phase space for this decay, yields the momentum distribution in Fig. 8 that can be observed experimentally in the heavy-quark limit. The maximum is in the mid-momentum region where phase space is larger and the wavefunction is near a local maximum.

However, since quarks are not infinitely heavy, the FC signature will be modified by their recoil and for the above discussed decays, involving $c(b)$-quarks in the $D(B)$ meson, corrections to the momentum distribution will be of order $\frac{m_D - m_c}{m_c} \simeq 0.2$. For example, taking a quark relative momentum between 150 and 200 MeV inside the daughter meson, one obtains the $c\bar{c}g$ momentum distribution illustrated in Fig. 9 for the ground state vector hybrid and the smeared final state $D\bar{D}$ momentum distribution plotted in Fig. 10 for radially excited charmonium. As can be seen, even after smearing there is still residual structure information adjacent to the central peak for radially excited charmonium that is reminiscent of its parent charmonium wavefunction behavior, in sharp contrast to the smooth, bell-shaped hybrid distribution. Other corrections involving the lighter π emission are similarly expected to be of this order and a more complete analysis would be worthwhile especially in the context of non-relativistic-QCD [52].

We therefore advocate analyzing the $D\bar{D}$ and $B\bar{B}$ relative momentum distributions in $D\bar{D}\pi$ and $B\bar{B}\pi$ decays of highly excited quarkonia. Additional final state pions or other light particles do not alter our arguments (but restrict somewhat the available phase space), so there are several other possible final state channels to search.

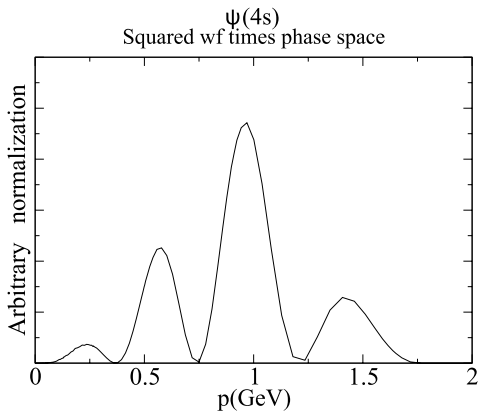

Fig. 8. Momentum distribution of Fig. 6 multiplied by the phase space for the decay $\psi(4260) \to D\bar{D}\pi$. This is the probability density for finding a $D\bar{D}\pi$ state with relative $D\bar{D}$ momentum p according to the Franck–Condon principle in the heavy-quark limit. This signature will be more robust for the related bottomonium process $\Upsilon(5s) \to B\bar{B}\pi$

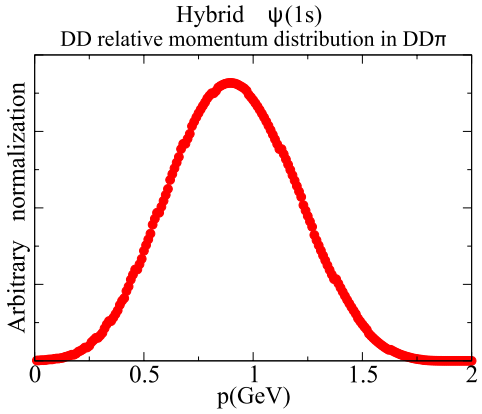

Fig. 9. The relative momentum distribution of the $D\bar{D}$ pair in the $D\bar{D}\pi$ final state for a charmed hybrid meson with momentum distribution given in Fig. 7. The distribution of the final products has a smooth bell shape, in sharp contrast to the radially excited quarkonium distribution in Fig. 10

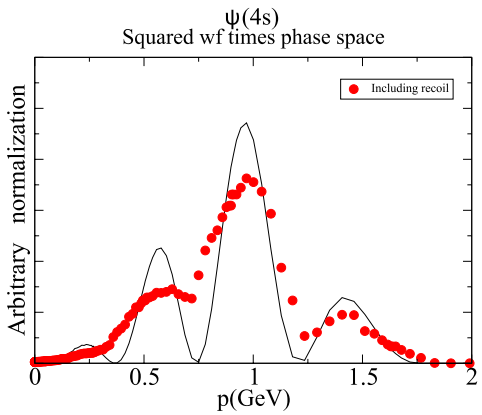

Fig. 10. The momentum distribution in Fig. 8 (*solid line*) and the distribution (*dots*) obtained averaging over a 150 MeV spread to approximate the actual quark momentum distribution in the D meson. The experimental signal, firmer for bottomonium than for charmonium, is a central peak with two shoulders for the relative momentum distribution of the $B\bar{B}$ (or $D\bar{D}$) pair in the $B\bar{B}\pi$ (or $D\bar{D}\pi$) final state. These adjacent enhancements identify the resonance as a radially excited quarkonium state as opposed to a hybrid meson

8 Discussion and conclusions

Our key model predictions are that the lightest hybrid mass is 2.1 GeV, with the lightest 1^{-+} exotic state slightly above 2.2 GeV. Lattice and flux tube calculations generally yield a mass of at least 1.8 GeV for the 1^{-+}. Thus, the composite model analyses appear to preclude the possibility of the reported 1^{-+} exotica, $\pi_1(1400)$ and $\pi_1(1600)$, being hybrid mesons. If this is correct, one should investigate other structures for those two hadrons, such as tetraquark molecules, with both $q\overline{q}$ pairs in color singlets, or tetraquark atoms, where quark pairs are in intermediate non-singlet color states, and we are currently applying our model to these systems. We note that one lattice 1^{-+} pre-

diction [18] is as low as 1.7 GeV, which does not exclude the observed $\pi_1(1600)$ from being a hybrid, but this still does not explain the structure of the $\pi_1(1400)$. It would be very useful to have other lattice measurements, using the same parameters as [18], to confirm or reject this result, we have also varied our model parameters and potential forms to obtain a lower bound for our predicted exotic hybrid mass, which is clearly above 2 GeV.

Regarding isospin splitting, our results show an enhanced splitting from g^2 corrections. For the 0^{++} hybrid, the corrections increased the splitting from 15 to 35 MeV, the maximum increase in the light hybrid spectrum.

In the strange sector, we predict the lightest non-exotic hybrid mass is 2.125 GeV, while the lightest exotic mass is 2.30 GeV. These values compare reasonably well with flux tube [20–22] and, slightly lighter, lattice [18] results. For the charmed sector, our predictions of 3.83 GeV for the lightest hybrid and 4.02 GeV for the lowest exotic are also in good agreement with several other lattice and flux tube studies (see Table 1).

As mentioned above, the different g^2 corrections produced an overall small effect, about the same order as the Monte Carlo error. However, the hyperfine correction becomes important for a heavier quark mass. In the charmed sector, this correction added about 500 to 600 MeV to the hybrid mass. Lastly, note that the level orderings of the exotic isoscalar $u\overline{u}g$ and $s\overline{s}g$ spectra are the same, 0^{--}, 1^{-+}, 1^{-+}, 1^{-+} and 3^{-+}, but slightly different than the exotic $c\overline{c}g$ system, where the 0^{--} and lowest 1^{-+} are degenerate. This is a consequence of the enhanced charmonium self-energy from the hyperfine interaction.

Finally, we discussed how the Frank–Condon principle provides a useful constraint on the final state momentum distributions following decay, which should assist experimentalists in identifying heavy hybrid systems.

In summary, lattice, flux tube and our $H_{\rm eff}$ many-body approach all yield similar hybrid spectra and predict that the lightest 1^{-+} exotic hybrid meson mass is near 2 GeV. This composite model agreement indicates that the $\pi_1(1600)$ is not a hybrid meson but has an alternative structure. If this is true and if the $\pi_1(1600)$ exists, it is more likely a tetraquark system, either a $(q\overline{q})$ $(q\overline{q})$ meson molecule or an exotic $qq\bar{q}\bar{q}$ atom. Future work will apply our model to light and heavy tetraquark systems including mixing with hybrid and conventional meson states. Three-body forces [51] will also be examined.

Acknowledgements. Work supported in part by grants FPA 2004-02602, 2005-02327, PR27/05-13955-BSCH (Spain) and U. S. DOE Grants DE-FG02-97ER41048 and DE-FG02-03ER41260.

References

1. D. Alde et al., Phys. Lett. B **205**, 397 (1988)
2. E852 Collaboration, D.R. Thompson et al., Phys. Rev. Lett. **79**, 1630 (1997)
3. E852 Collaboration, S.U. Chung et al., Phys. Rev. D **60**, 092 001 (1999)
4. E852 Collaboration, G.S. Adams et al., Phys. Rev. Lett. **81**, 5760 (1998)
5. E852 Collaboration, S.U. Chung et al., Phys. Rev. D **65**, 072 001 (2002)
6. A.R. Dzierba et al., Phys. Rev. D **73**, 072 001 (2006)
7. VES Collaboration, D.V. Amelin et al., Phys. Lett. B **356**, 595 (1995)
8. A. Zaitsev, AIP Conf. Proc. **432**, 461 (1998)
9. A. Donnachie, Y.S. Kalashnikova, Phys. Rev. D **60**, 114 011 (1999)
10. Crystal Ball Collaboration, K. Karch et al., Z. Phys. C **54**, 33 (1992)
11. Crystal Barrel Collaboration, J. Adomeit et al., Z. Phys. C **71**, 227 (1996)
12. WA102 Collaboration, D. Barberis et al., Phys. Lett. B **413**, 217 (1997)
13. Y.S. Kalashnikova, Nucl. Phys. A **689**, 49 (2001)
14. F. Buisseret, V. Mathieu, arXiv:hep-ph/0607083
15. C. Bernard et al., Phys. Rev. D **56**, 7039 (1997)
16. C. Bernard et al., Nucl. Phys. B Proc. Suppl. **73**, 264 (1999)
17. P. Lacock, K. Schilling, Nucl. Phys. B Proc. Suppl. **73**, 261 (1999)
18. J.N. Hedditch et al., Phys. Rev. D **72**, 114 507 (2005)
19. X.Q. Luo, Z.H. Mei, Nucl. Phys. B Proc. Suppl. **119**, 263 (2003)
20. T. Barnes, F.E. Close, E.S. Swanson, Phys. Rev. D **52**, 5242 (1995)
21. F.E. Close, P.R. Page, Nucl. Phys. B **443**, 233 (1995)
22. K. Waidelich, Diploma Thesis, North Carolina State University (2001)
23. T. Barnes, Ph.D. Thesis, Caltech (1977)
24. T. Barnes, Nucl. Phys. B **158**, 171 (1979)
25. T. Barnes, F. Close, Phys. Lett. B **116**, 365 (1982)
26. M. Chanowitz, S. Sharpe, Nucl. Phys. B **222**, 211 (1983)
27. T. Barnes et al., Nucl. Phys. B **224**, 241 (1983)
28. M. Flensburg et al., Z. Phys. C **22**, 293 (1984)
29. P. Hasenfratz et al., Phys. Lett. B **95**, 299 (1980)
30. F. Iddir, L. Semlala, arXiv:hep-ph/0511086
31. Y. Liu, X.Q. Luo, Phys. Rev. D **73**, 054 510 (2006)
32. L.A. Griffiths, C. Michael, P.E.L. Rakow, Phys. Lett. B **129**, 351 (1983)
33. S. Perantonis, C. Michael, Nucl. Phys. B **347**, 854 (1990)
34. F.J. Llanes-Estrada, S.R. Cotanch, Nucl. Phys. A **697**, 303 (2002)
35. F.J. Llanes-Estrada, S.R. Cotanch, A.P. Szczepaniak, E.S. Swanson, Phys. Rev. C **70**, 035 202 (2004)
36. F.J. Llanes-Estrada, P. Bicudo, S.R. Cotanch, Phys. Rev. Lett. **96**, 081 601 (2006)
37. F.J. Llanes-Estrada, S.R. Cotanch, Phys. Rev. Lett. **84**, 1102 (2000)
38. G.S. Bali, K. Schilling, Phys. Rev. D **46**, 2636 (1992)
39. J. Greensite, S. Olejnik, Phys. Rev. D **67**, 094 503 (2003) [arXiv:hep-lat/0302018]
40. D. Zwanziger, Phys. Rev. D **70**, 094 034 (2004) [arXiv:hep-ph/0312254]
41. K. Langfeld, L. Moyaerts, Phys. Rev. D **70**, 074 507 (2004) [arXiv:hep-lat/0406024]
42. E. Gubankova, C.R. Ji, S.R. Cotanch, Phys. Rev. D **62**, 074 001 (2000) [arXiv:hep-ph/0003289]
43. D.G. Robertson, E.S. Swanson, A.P. Szczepaniak, C.R. Ji, S.R. Cotanch, Phys. Rev. D **59**, 074 019 (1999)

44. F.J. Llanes-Estrada, S.R. Cotanch, Phys. Lett. B **504**, 15 (2001)
45. T.D. Lee, Particle Physics and Introduction to Field Theory (Harwood Academic Publishers, New York, 1990)
46. D. Zwanziger, Nucl. Phys. B **485**, 185 (1997) and private communication
47. A.P. Szczepaniak, E.S. Swanson, Phys. Rev. D **65**, 0 252 012 (2002)
48. G.P. Lepage, J. Comput. Phys. **27**, 192 (1978)
49. G.P. Lepage, Cornell University Report CLNS (1980) 80–447 (unpublished)
50. S. Eidelman et al., Phys. Lett. B **592**, 1 (2004)
51. A.P. Szczepaniak, P. Krupinski, Phys. Rev. D **73**, 116 002 (2006)
52. Joan Soto, private communication at Brookhaven National Laboratory's "International Heavy Quarkonium Workshop", June 2006